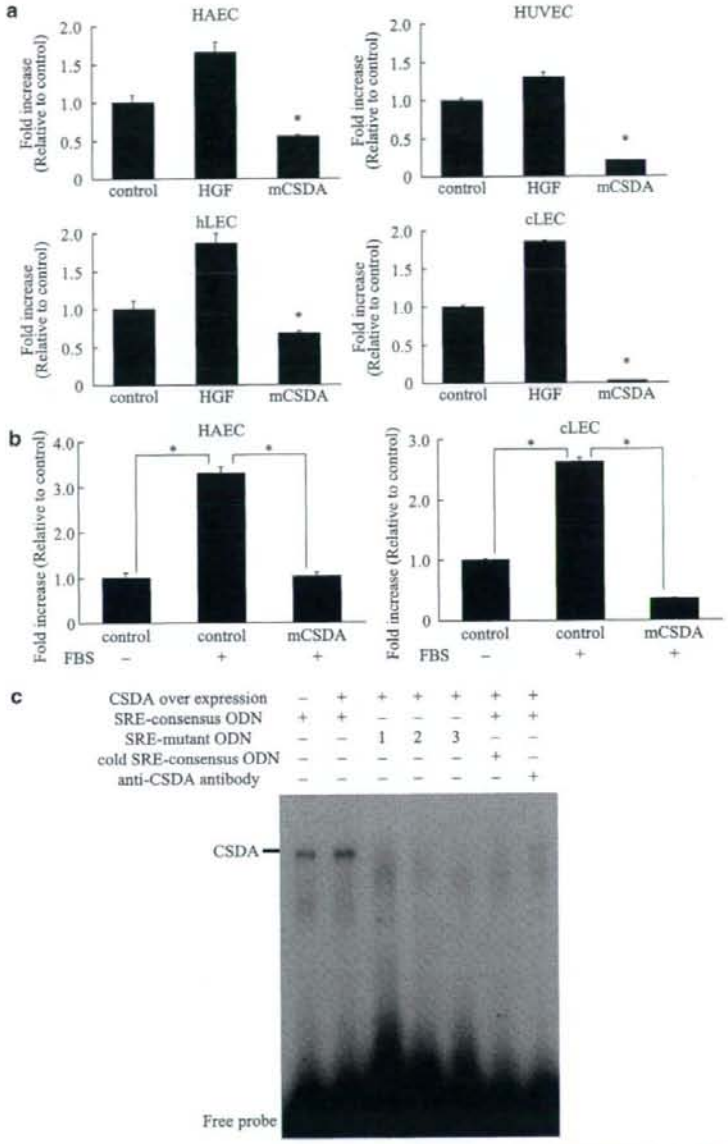

Figure 6 Repression of serum response element by mouse cold shock domain protein A (mCSDA) in ECs. (**a**) Effect of mCSDA plasmid on SRE activity in human aortic endothelial cells (HAEC), human umbilical vein endothelial cell (HUVEC), hLEC and canine lymphatic endothelial cells (cLEC). GFP plasmid was transfected as control, and hepatocyte growth factor (HGF) plasmid was transfected as positive control ($n=8$, $^*P<0.05$ vs control). (**b**) Effect of mCSDA plasmid with or without fetal bovine serum (FBS) on HAEC and cLEC, as demonstrated by the SRE assay. ECs were transfected with mCSDA plasmid or GFP plasmid as control and then cultured in FBS-free medium (FBS −) or 10% FBS medium (FBS +) ($n=8$, $^*P<0.05$ vs control). (**c**) Representative image of gel retardation assay for CSDA binding to SRE.

dye in intratumor that can selectively stain the lymphatic vessels. On the control group tissue of footpad model, the lymph node at inguinal region was rapidly stained after intratumoral injection of patent blue, while in the CSDA group, the dye did not drain from tumor for a long period of time (Figure 9d). Indeed, inguinal lymph node metastasis of

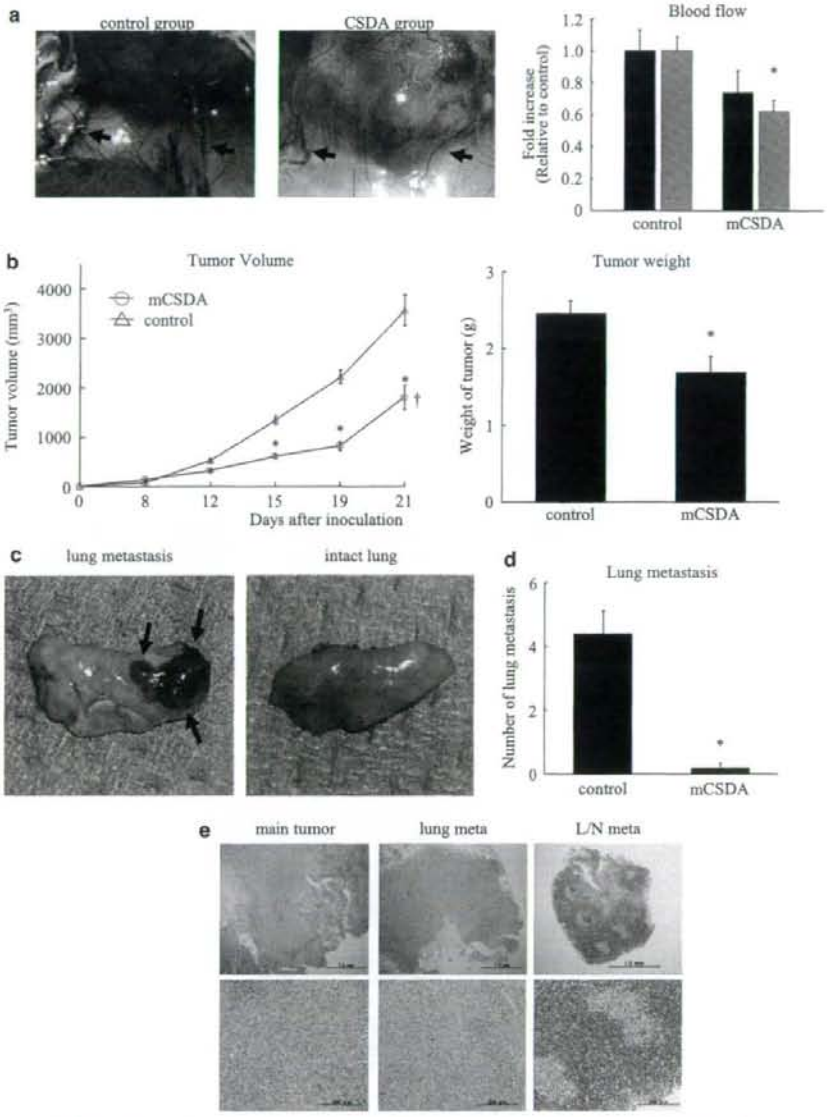

Figure 7 Cold shock domain protein A (CSDA) inhibits tumor growth and lung metastasis. (**a**) Macroscopic appearance of main tumor (left and middle panels). Arrows indicate the feeding arteries. Effect of mouse cold shock domain protein A (mCSDA) transfection on blood flow on day 21 after inoculation (black bar; blood flow within tumor, gray bar; blood flow around tumor). $n=10$, $^{*}P<0.01$ vs control (right panel). (**b**) Effect of mCSDA transfection on tumor volume, on days 0, 8, 12, 15, 19 and 21 after inoculation ($n=10$, $^{*}P<0.01$ vs control; $^{\dagger}P<0.0001$ vs the area under the effect curve (AUEC) of control (left panel)). Effect of mCSDA transfection on tumor weight on day 21 after inoculation ($n=10$, $^{*}P<0.05$ vs control (right panel)). (**c**) Macroscopic appearance of metastatic tumor (left panel) and intact (right panel) lung. Arrows indicate the metastasis tumor. (**d**) Effect of mCSDA transfection on lung metastasis on day 21 after inoculation ($n=10$, $^{*}P<0.001$ vs control). (**e**) Representative H&E staining of main tumor (left panels), lung metastasis (middle panels) and lymph node metastasis (right panels). Upper panels, × 40 magnification; lower panels, × 200 magnification.

footpad model was decreased in the CSDA group compared with the control group (frequency, control group: 7/11 (63.6%); CSDA group: 1/7 (14.3%)), and luciferase activity of lymph node was significantly decreased in the CSDA group compared with the control group ($P<0.05$; Figure 9e).

These data strongly suggested that overexpressed CSDA repressed the growth and metastasis of LL/2 by the antiangiogenic and antilymphangiogenic effect.

Discussion

Inhibition of angiogenesis or lymphangiogenesis is a promising strategy for treatment of cancer, and cancer cells shed from a primary tumor via two major routes, blood and lymphatic vessels, to establish distant metastases. In terms of antiangiogenic or antilymphangiogenic therapy, at least three strategies are feasible: (1) inhibition of the release of angiogenic or lymphangiogenic molecules from tumor cells, that is, inhibition of HIF-1; (2) neutralization of angiogenic or lymphangiogenic molecules that are released from tumors, that is, anti-VEGF antibody (bevacizumab) (Hurwitz *et al.*, 2004), VEGF165 aptamer (pegaptanib) (Gragoudas *et al.*, 2004) and soluble VEGFR-3-Ig fusion protein (Karpanen *et al.*, 2001) and (3) blockade of the vascular EC response to angiogenic or lymphangiogenic stimulation, that is, endostatin (O'Reilly *et al.*, 1997), tumstatin (Sund *et al.*, 2005), vasostatin (Pike *et al.*, 1998) and vasohibin (Watanabe *et al.*, 2004). Although many antiangiogenic or -lymphangiogenic agents have been reported, these agents were limited of the effect because of a great variety of malignancies. We speculate that blockade of one molecule in above three strategies is not enough to fight against cancer cells though antiangiogenesis and antilymphangiogenesis therapy, because some cancer cells may overcome the blockade and rapidly grow. Here, we demonstrate the first report of a multifunctional gene that represses both angiogenesis and lymphangiogenesis, which potentially inhibits VEGF-A promoter activity (Strategy 1) and directly represses vascular and lymphatic EC proliferation via repression of SRE activity (Strategy 3).

Negative regulation is an important physiological mechanism that controls a wide range of phenomena (Lord, 1988). Folkman (2006) hypothesized that if tumors produce both stimulators and inhibitors of angiogenesis, the stimulators (that is, VEGF) could accumulate in excess of inhibitors within an angiogenic tumor and emergence of tumor angiogenesis was the result of a shift in balance between positive and negative regulators of angiogenesis in a tumor. Thus, the present study screened an LL/2-derived cDNA library to characterize negative regulators of angiogenesis and lymphangiogenesis, as LL/2 cells may form hypervascular tumors and induce metastasis.

Cold shock domain proteins (also called Y-box proteins) repress growth factor and stress response genes via DNA-binding and non-DNA-binding mechanisms (Shannon *et al.*, 1997, 2001). CSDA binds to CT-rich sequences, such as the HRE of the VEGF-A promoter, which subsequently binds to the HIF-1 transcription factor and represses the VEGF-A promoter in normoxic fibroblasts (Coles *et al.*, 2002). This results in the formation of a CSD protein nuclear complex (Coles *et al.*, 1996; Diamond *et al.*, 2001) that may contribute to antiangiogenesis. In contrast, antilymphangiogenesis may require modulation of VEGF-C, as VEGF-C is a common growth factor for lymphatic ECs (VEGF-A is slightly concerned with lymphangiogenesis), and the VEGF-C promoter does not contain an HRE. Thus, the present study focused on the SRE as a target CSDA-binding sequence. As shown in Figure 5c, the ras/ERK pathway provides a common route by which signals from different growth factor receptors converge at a major regulatory element of the promoters of the c-*fos* and other coregulated genes via the SRE (Hill *et al.*, 1994). By virtue of its ability to bind to the SRE and compete with Elk-1, CSDA inhibits VEGF-A and VEGFR-2 signaling as well as other signaling pathways mediated by various growth factors, such as VEGF-C, fibroblast growth factor-2 and HGF (Rikitake *et al.*, 2000; Nakagami *et al.*, 2001). Indeed, inhibition of SRE activation by CSDA represses both angiogenesis and lymphangiogenesis.

In conclusion, the present study demonstrated that gene transfer of CSDA plasmid DNA into ECs repressed both angiogenesis and lymphangiogenesis *in vitro* and *in vivo*. These data may help guide the development of novel therapeutics to concomitantly inhibit angiogenesis and lymphangiogenesis in the context of various malignancies.

Materials and methods

Cell culture

HAEC, HUVEC and HASMC were maintained as previously described (Nakagami *et al.*, 2001). BAEC, BHK-21 and COS-7 were maintained in Dulbecco's modified Eagle medium containing 10% FBS, 100 U ml^{-1} penicillin and 100 μg ml^{-1} streptomycin. Human LEC (neonatal dermis) and cLEC that were isolated from canine thoracic ducts as previously described (Saito *et al.*, 2006) were maintained in EBM-2 medium supplemented with 20% FBS and endothelial growth supplement on 0.1% gelatin-coated culture dishes. Cultures were incubated at 37 °C in a humidified atmosphere of 95% air–5% CO_2 with exchange of medium every 2 days. These cells were used at passages 5–8 for subsequent experimental protocols. Cells were transfected using Lipofectamine2000 Transfection Reagent (Invitrogen, Carlsbad, CA, USA).

Establishment of LL/2 stable transfectant expressing luciferase

LL/2 cells were plated into six-well plates and transfected with 4 μg per well of pcDNA3.1-luciferase plasmid using Lipofectamine2000 Transfection Reagent (Invitrogen). After 48 h of transfection, the cells were passaged and cultured in medium supplemented with Geneticin (G418) at 400 μg ml^{-1} for 4 weeks. Stably transfected clones (LL/2/Luc) were picked and maintained in medium containing G418 for additional studies.

cDNA library and functional screening using HVJ-E

Functional screening of cDNA library using HVJ-E vector was performed as previously described (Nishikawa *et al.*, 2006). First, cDNA library was made from LL/2 as previously described (Kobori *et al.*, 1998), which was amplified once using the Plasmid Giga Kit (Qiagen, Valencia, CA, USA), and infused into HVJ-E vectors as previously described (Kaneda *et al.*, 2002). Briefly, BHK-21 were seeded on 100-mm dishes and

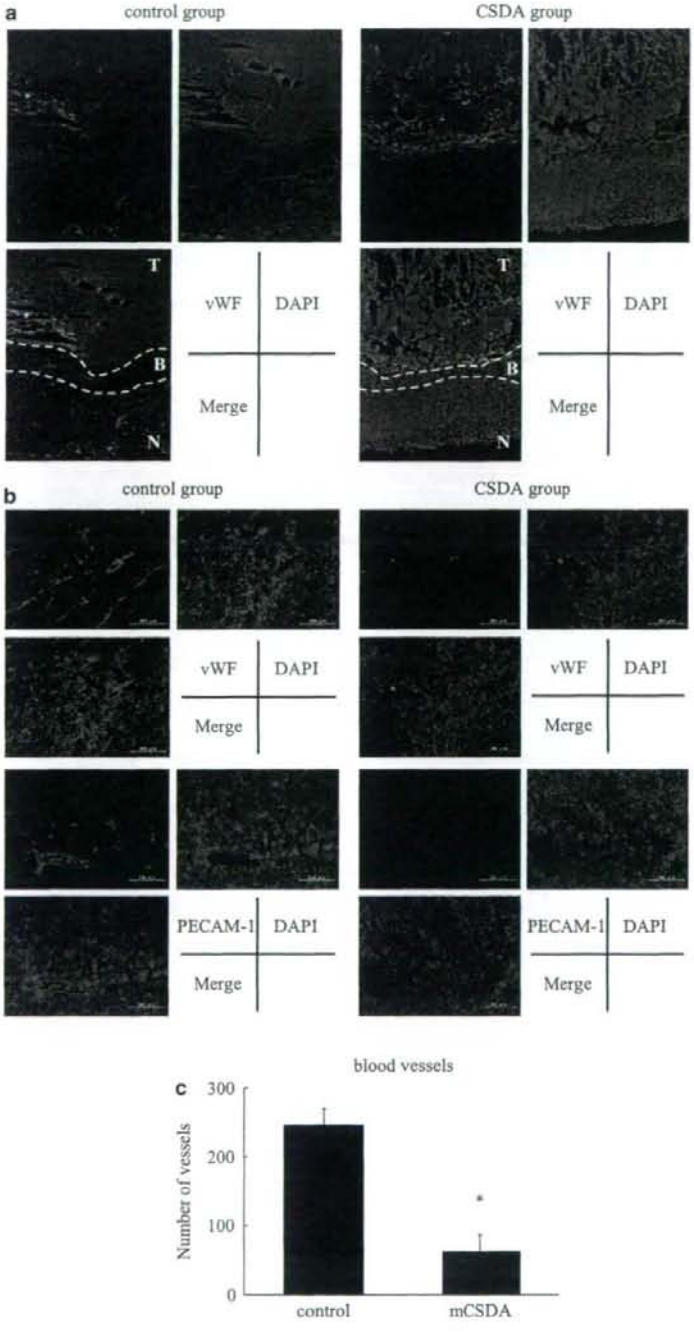
a
control group
CSDA group
T
B
N
vWF
DAPI
Merge
b
control group
CSDA group
vWF
DAPI
Merge
PECAM-1
DAPI
Merge
blood vessels
c
Number of vessels
300
200
100
0
control
mCSDA
*

transfected with cDNA library-infused HVJ-E and then cocultured with cLEC using Falcon Cell Culture Inserts (Becton Dickinson Labware, Franklin Lakes, NJ, USA) for 48 h. Candidate genes were obtained from BHK-21 cells with the lowest on MTS assay values using CellTiter 96 One Solution Reagent on cLEC (Promega, Madison, WI, USA), as previously described (Nakagami *et al.*, 2005), followed by isolation of transfected genes by transformation into *Escherichia coli*.

Gene transfer protocol for antiangiogenesis and antilymphangiogenesis therapy

Male C57BL/6 mice (5–6 weeks old; Oriental Yeast Co. Ltd, Tokyo, Japan) were inoculated intradermally with 5×10^6 LL/2 cells. Twenty mice were injected in the right hind flank (flank model) with normal LL/2 cells, and 10 mice were injected in the footpad of there hind leg (footpad model) with LL/2/Luc cells. In total, 30 model mice were randomly assigned to one of two groups: mCSDA plasmid (200 μg per 0.1 ml; inserted on pcDNA3.1) and GFP plasmid (200 μg per 0.1 ml; inserted on pcDNA3.1). Mouse CSDA or GFP plasmid was injected subcutaneously at the boundary area between tumor and normal tissue (Figures 8a and 9a; inside of white dotted lines) using a 30-gauge needle on days 8, 12, 15 and 19 after inoculation. Injected plasmids were transfected using a microbubble-enhanced ultrasound method, as previously described (Shimamura *et al.*, 2004).

Tumor size was evaluated periodically, and the tumor volume was calculated as length × width^2 × 0.5. Blood flow by laser Doppler imaging (Moor Instruments, Devon, UK) and capillary density within the tumor or around the tumor was assessed for analysis of angiogenesis as previously described (Taniyama *et al.*, 2001). At day 21, 0.2 ml of 0.5% patent blue was injected into the tumor in the footpad model mice for visualization of lymphatic vessels and lymph nodes based on the sentinel node navigation concept. Then all animals were killed and frozen sections were prepared from the excised tissues including the main tumor and connecting normal tissue. Blood or lymphatic vessel quantification was performed by assessing positive immunofluorescent staining for anti-vWF and LYVE-1 in five randomly selected fields as previously described (Yoon *et al.*, 2003).

All animal protocols were approved by the Animal Ethics Committee of Asahikawa Medical University and by the Osaka University Committee on Animal Research.

Other methods used in this study are described in the Supplementary Methods.

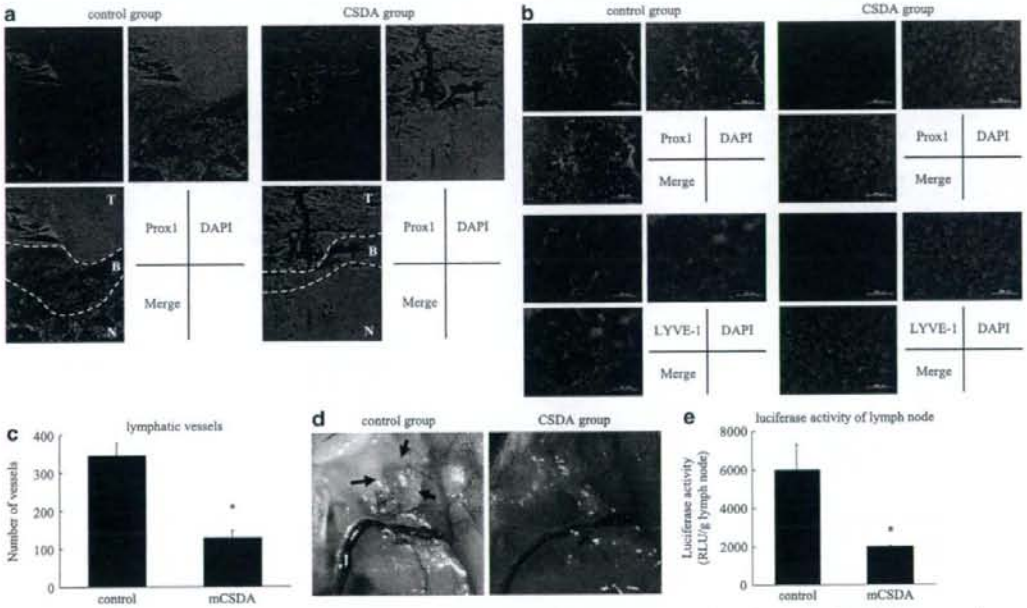

Figure 9 Cold shock domain protein A (CSDA) inhibits lymphangiogenesis and lymph node metastasis. (**a**) Representative immunofluorescent staining image for the lymphatic endothelial cells marker (Prox1). T, tumor; N, normal tissue; B (inside of white dotted lines), the boundary area between tumor and normal tissue (× 40 magnification). (**b**) Magnification images of the boundary area (× 200 magnification). Endothelial cells marker (Prox1, LYVE-1); red, DAPI; blue. (**c**) Quantitative analysis of stained lymphatic vessels (LYVE-1) in each group ($n = 5$, $^*P < 0.05$ vs control). (**d**) Macroscopic appearance of inguinal region. Arrows indicate the inguinal lymph node stained by patent blue. (**e**) Effect of mouse cold shock domain protein A (mCSDA) transfection on lymph node luciferase activity on day 21 after inoculation ($n = 5$, $^*P < 0.05$ vs control).

Figure 8 Cold shock domain protein A (CSDA) inhibits angiogenesis. (**a**) Representative immunofluorescent staining image for the vascular endothelial cell marker vWF (von Willebrand factor). T, tumor; N, normal tissue; B (inside of white dotted lines), the boundary area between tumor and normal tissue (× 40 magnification). (**b**) Magnification images of the boundary area (× 200 magnification). Endothelial cells marker (vWF, PECAM-1); red, DAPI; blue. (**c**) Quantitative analysis of stained blood vessels (vWF) in each group ($n = 5$, $^*P < 0.01$ vs control).

Acknowledgements

This work was supported by the Northern Osaka (Saito) Biomedical Knowledge-Based Cluster Creation Project and the Mitsubishi Pharma Research Foundation. We thank Prof. Hiroshi Nojima of Osaka University for technical assistance and advice in making cDNA library and Dr Gregory J Goodall of the Hanson Centre for Cancer Research, Institute of Medicine and Veterinary Science for providing the hCSDA plasmid.

References

Akagi K, Ikeda Y, Miyazaki M, Abe T, Kinoshita J, Maehara Y *et al.* (2000). Vascular endothelial growth factor-C (VEGF-C) expression in human colorectal cancer tissues. *Br J Cancer* **83**: 887–891.

Bergers G, Song S, Meyer-Morse N, Bergsland E, Hanahan D. (2003). Benefits of targeting both pericytes and endothelial cells in the tumor vasculature with kinase inhibitors. *J Clin Invest* **111**: 1287–1295.

Bunone G, Vigneri P, Mariani L, Buto S, Collini P, Pilotti S *et al.* (1999). Expression of angiogenesis stimulators and inhibitors in human thyroid tumors and correlation with clinical pathological features. *Am J Pathol* **155**: 1967–1976.

Chilov D, Kukk E, Taira S, Jeltsch M, Kaukonen J, Palotie A *et al.* (1997). Genomic organization of human and mouse genes for vascular endothelial growth factor C. *J Biol Chem* **272**: 25176–25183.

Coles LS, Diamond P, Lambrusco L, Hunter J, Burrows J, Vadas MA *et al.* (2002). A novel mechanism of repression of the vascular endothelial growth factor promoter, by single strand DNA binding cold shock domain (Y-box) proteins in normoxic fibroblasts. *Nucleic Acids Res* **30**: 4845–4854.

Coles LS, Diamond P, Occhiodoro F, Vadas MA, Shannon MF. (1996). Cold shock domain proteins repress transcription from the GM-CSF promoter. *Nucleic Acids Res* **24**: 2311–2317.

Diamond P, Shannon MF, Vadas MA, Coles LS. (2001). Cold shock domain factors activate the granulocyte-macrophage colony-stimulating factor promoter in stimulated Jurkat T cells. *J Biol Chem* **276**: 7943–7951.

Folkman J. (1971). Tumor angiogenesis: therapeutic implications. *N Engl J Med* **285**: 1182–1186.

Folkman J. (2006). Antiangiogenesis in cancer therapy—endostatin and its mechanisms of action. *Exp Cell Res* **312**: 594–607.

Gragoudas ES, Adamis AP, Cunningham Jr ET, Feinsod M, Guyer DR. (2004). Pegaptanib for neovascular age-related macular degeneration. *N Engl J Med* **351**: 2805–2816.

Hill CS, Wynne J, Treisman R. (1994). Serum-regulated transcription by serum response factor (SRF): a novel role for the DNA binding domain. *EMBO J* **13**: 5421–5432.

Hurwitz H, Fehrenbacher L, Novotny W, Cartwright T, Hainsworth J, Heim W *et al.* (2004). Bevacizumab plus irinotecan, fluorouracil, and leucovorin for metastatic colorectal cancer. *N Engl J Med* **350**: 2335–2342.

Izumi Y, Xu L, di Tomaso E, Fukumura D, Jain RK. (2002). Tumour biology: herceptin acts as an anti-angiogenic cocktail. *Nature* **416**: 279–280.

Kaneda Y, Nakajima T, Nishikawa T, Yamamoto S, Ikegami H, Suzuki N *et al.* (2002). Hemagglutinating virus of Japan (HVJ) envelope vector as a versatile gene delivery system. *Mol Ther* **6**: 219–226.

Kaplan RN, Riba RD, Zacharoulis S, Bramley AH, Vincent L, Costa C *et al.* (2005). VEGFR1-positive haematopoietic bone marrow progenitors initiate the pre-metastatic niche. *Nature* **438**: 820–827.

Karpanen T, Egeblad M, Karkkainen MJ, Kubo H, Yla-Herttuala S, Jaattela M *et al.* (2001). Vascular endothelial growth factor C promotes tumor lymphangiogenesis and intralymphatic tumor growth. *Cancer Res* **61**: 1786–1790.

Kim KJ, Li B, Winer J, Armanini M, Gillett N, Phillips HS *et al.* (1993). Inhibition of vascular endothelial growth factor-induced angiogenesis suppresses tumour growth *in vivo*. *Nature* **362**: 841–844.

Kobori M, Ikeda Y, Nara H, Kato M, Kumegawa M, Nojima H *et al.* (1998). Large scale isolation of osteoclast-specific genes by an improved method involving the preparation of a subtracted cDNA library. *Genes Cells* **3**: 459–475.

Kudo S, Mattei MG, Fukuda M. (1995). Characterization of the gene for dbpA, a family member of the nucleic-acid-binding proteins containing a cold-shock domain. *Eur J Biochem* **231**: 72–82.

Lord BI. (1988). Feedback regulators in normal and tumour tissues. *J Cell Sci* **10**(Suppl): 231–242.

Mandriota SJ, Jussila L, Jeltsch M, Compagni A, Baetens D, Prevo R *et al.* (2001). Vascular endothelial growth factor-C-mediated lymphangiogenesis promotes tumour metastasis. *EMBO J* **20**: 672–682.

Nakagami H, Maeda K, Morishita R, Iguchi S, Nishikawa T, Takami Y *et al.* (2005). Novel autologous cell therapy in ischemic limb disease through growth factor secretion by cultured adipose tissue-derived stromal cells. *Arterioscler Thromb Vasc Biol* **25**: 2542–2547.

Nakagami H, Morishita R, Yamamoto K, Taniyama Y, Aoki M, Matsumoto K *et al.* (2001). Mitogenic and antiapoptotic actions of hepatocyte growth factor through ERK, STAT3, and AKT in endothelial cells. *Hypertension* **37**: 581–586.

Niki T, Iba S, Tokunou M, Yamada T, Matsuno Y, Hirohashi S. (2000). Expression of vascular endothelial growth factors A, B, C, and D and their relationships to lymph node status in lung adenocarcinoma. *Clin Cancer Res* **6**: 2431–2439.

Nishikawa T, Nakagami H, Matsuki A, Maeda A, Yo CY, Harada T *et al.* (2006). Development of high-throughput functional screening of therapeutic genes, using a hemagglutinating virus of Japan envelope vector. *Hum Gene Ther* **17**: 470–475.

O'Reilly MS, Boehm T, Shing Y, Fukai N, Vasios G, Lane WS *et al.* (1997). Endostatin: an endogenous inhibitor of angiogenesis and tumor growth. *Cell* **88**: 277–285.

Pepper MS. (2001). Lymphangiogenesis and tumor metastasis: myth or reality? *Clin Cancer Res* **7**: 462–468.

Pike SE, Yao L, Jones KD, Cherney B, Appella E, Sakaguchi K *et al.* (1998). Vasostatin, a calreticulin fragment, inhibits angiogenesis and suppresses tumor growth. *J Exp Med* **188**: 2349–2356.

Rikitake Y, Kawashima S, Yamashita T, Ueyama T, Ishido S, Hotta H *et al.* (2000). Lysophosphatidylcholine inhibits endothelial cell migration and proliferation via inhibition of the extracellular signal-regulated kinase pathway. *Arterioscler Thromb Vasc Biol* **20**: 1006–1012.

Saito Y, Nakagami H, Morishita R, Takami Y, Kikuchi Y, Hayashi H *et al.* (2006). Transfection of human hepatocyte growth factor gene ameliorates secondary lymphedema via promotion of lymphangiogenesis. *Circulation* **114**: 1177–1184.

Shannon MF, Coles LS, Attema J, Diamond P. (2001). The role of architectural transcription factors in cytokine gene transcription. *J Leukoc Biol* **69**: 21–32.

Shannon MF, Coles LS, Vadas MA, Cockerill PN. (1997). Signals for activation of the GM-CSF promoter and enhancer in T cells. *Crit Rev Immunol* **17**: 301–323.

Shimamura M, Sato N, Taniyama Y, Yamamoto S, Endoh M, Kurinami H *et al.* (2004). Development of efficient plasmid DNA transfer into adult rat central nervous system using microbubble-enhanced ultrasound. *Gene Therapy* **11**: 1532–1539.

Skobe M, Hawighorst T, Jackson DG, Prevo R, Janes L, Velasco P *et al.* (2001). Induction of tumor lymphangiogenesis by VEGF-C promotes breast cancer metastasis. *Nat Med* **7**: 192–198.

Sleeman JP. (2000). The lymph node as a bridgehead in the metastatic dissemination of tumors. *Recent Results Cancer Res* **157**: 55–81.

Stacker SA, Caesar C, Baldwin ME, Thornton GE, Williams RA, Prevo R *et al.* (2001). VEGF-D promotes the metastatic spread of tumor cells via the lymphatics. *Nat Med* **7**: 186–191.

Sund M, Hamano Y, Sugimoto H, Sudhakar A, Soubasakos M, Yerramalla U *et al.* (2005). Function of endogenous inhibitors of angiogenesis as endothelium-specific tumor suppressors. *Proc Natl Acad Sci USA* **102**: 2934–2939.

Taniyama Y, Morishita R, Aoki M, Nakagami H, Yamamoto K, Yamazaki K *et al.* (2001). Therapeutic angiogenesis induced by human hepatocyte growth factor gene in rat and rabbit hindlimb ischemia models: preclinical study for treatment of peripheral arterial disease. *Gene Therapy* **8**: 181–189.

Tsurusaki T, Kanda S, Sakai H, Kanetake H, Saito Y, Alitalo K *et al.* (1999). Vascular endothelial growth factor-C expression in human prostatic carcinoma and its relationship to lymph node metastasis. *Br J Cancer* **80**: 309–313.

Watanabe K, Hasegawa Y, Yamashita H, Shimizu K, Ding Y, Abe M *et al.* (2004). Vasohibin as an endothelium-derived negative feedback regulator of angiogenesis. *J Clin Invest* **114**: 898–907.

Yonemura Y, Endo Y, Fujita H, Fushida S, Ninomiya I, Bandou E *et al.* (1999). Role of vascular endothelial growth factor C expression in the development of lymph node metastasis in gastric cancer. *Clin Cancer Res* **5**: 1823–1829.

Yoon YS, Murayama T, Gravereaux E, Tkebuchava T, Silver M, Curry C *et al.* (2003). VEGF-C gene therapy augments postnatal lymphangiogenesis and ameliorates secondary lymphedema. *J Clin Invest* **111**: 717–725.

Zou W. (2005). Immunosuppressive networks in the tumour environment and their therapeutic relevance. *Nat Rev Cancer* **5**: 263–274.

Supplementary Information accompanies the paper on the Oncogene website (http://www.nature.com/onc).

Available online at www.sciencedirect.com
ScienceDirect
Journal of Biotechnology 133 (2008) 386–394
Journal of BIOTECHNOLOGY
www.elsevier.com/locate/jbiotec

Functional modification of Sendai virus by siRNA

Kotaro Saga, Katsuto Tamai, Masako Kawachi, Takashi Shimbo, Hiroshi Fujita, Takehiko Yamazaki, Yasufumi Kaneda *

Division of Gene Therapy Science, Graduate School of Medicine, Osaka University, 2-2 Yamada-oka, Suita, Osaka 565-0871, Japan

Received 26 March 2007; received in revised form 10 October 2007; accepted 23 October 2007

Abstract

Sendai virus (hemagglutinating virus of Japan; HVJ) is a negative-strand RNA virus with robust fusion activity, and has been utilized for gene transfer and drug delivery. Hemagglutinin-neuraminidase (HN) protein on the viral membrane is important for cell fusion, but causes agglutination of red blood cells. HN-depleted HVJ has been desired for *in vivo* transfection in order to improve safety. Here, we succeeded in producing HN-depleted HVJ using HN-specific short interfering RNA (siRNA). Viral production was not affected by the siRNA. HN protein was markedly decreased in the new HVJ, while other viral proteins were retained. Consequently, the hemagglutinating activity was substantially reduced and infection activity was suppressed. When the HN-depleted HVJ was mixed with cultured cells and the mixture was centrifuged for 10 min at 2000 × *g*, the modified HVJ recovered its infectivity to approximately 80% of wild HVJ. However, infectivity was abolished in the presence of anti-F antibody. Moreover, transfection of FITC-labeled oligodeoxynucleotides using the modified HVJ was also recovered by centrifugation. Thus, the HN-depleted HVJ produced using siRNA technology will be applicable to a delivery vector.

Keywords: Sendai virus; HVJ; siRNA; HN; Knock-down; Modification

1. Introduction

Sendai virus (hemagglutinating virus of Japan; HVJ) belongs to the paramyxovirus family, which has a negative-sense single-strand RNA genome (Curran and Kolakofsky, 1999; Lamb and Kolakofsky, 2001). The genome encodes six viral proteins: nucleocapsid (N), phospho (P), large (L), matrix (M), fusion (F) and hemagglutinin-neuraminidase (HN). Of these, HN and F are membrane glycoproteins on the HVJ envelope (Okada, 1993; Yeagle, 1993), and M binds to the cytoplasmic domain of these glycoproteins (Ali and Nayak, 2000; Mottet et al., 1999; Takimoto et al., 2001).

The F protein is translated as F_0 in host cells, and in principle, F_0 is activated in the trans Golgi, ensuring that F_1/F_2 is present in infectious viral progeny. In tissue culture cells lacking the furin-like protease; however, F_0 is not cleaved and the produced virion is not infectious (Tashiro et al., 1999). HN binds to sialic acid, its cell-surface receptor, and neuraminidase to degrade the receptor (Takimoto et al., 2002). Infection starts with the binding of HN to sialic acid and subsequent receptor degradation. F then induces membrane fusion by inserting its putative fusion peptide into the lipid bilayer of the cell membrane, facilitating viral genome introduction into the target cell (Asano and Asano, 1988).

The fusion activity of HVJ has been used to construct novel drug-delivery vectors. We recently succeeded in incorporating therapeutic molecules directly into inactivated HVJ particles without liposomes (Kaneda et al., 2002). The resulting HVJ-envelope vector (HVJ-E) enables delivery of proteins, synthetic oligonucleotides and drugs, as well as plasmid DNA, to target cells both *in vitro* and *in vivo* (Kaneda et al., 2005).

However, one of the limitations of these HVJ-derived vectors is hemagglutination and hemolysis of red blood cells (Inoue et al., 1985). Hemagglutination occurs when HN protein binds to sialic acid on the surface of red blood cells (Portner et al., 1987), while hemolysis is induced by both F and HN (Dallocchio et al., 1995; Hoekstra and Klappe, 1986). Therefore, regulation of HN expression on HVJ is necessary to develop less invasive vectors.

In order to address this issue, we report here successful regulation of HN activity on HVJ using HN-specific short interfering RNA (siRNA).

* Corresponding author. Tel.: +81 6 6879 3900; fax: +81 6 6879 3909.
E-mail address: kaneday@gts.med.osaka-u.ac.jp (Y. Kaneda).

0168-1656/$ – see front matter © 2007 Elsevier B.V. All rights reserved.
doi:10.1016/j.jbiotec.2007.10.003

2. Materials and methods

2.1. Virus

HVJ (VR-105 parainfluenza1 Sendai/52, Z strain) was purchased from American Type Culture Collection (Manassas, VA, USA), amplified in the chorioallantoic fluid of 10–14-day-old chick eggs, and purified by centrifugation, as described previously (Kaneda et al., 2002).

2.2. Antibodies

Mouse monoclonal antibody (IgG) against F protein, f236 (Tozawa et al., 1986) was kindly provided by H. Taira (Department of Bioscience and Technology, Faculty of Agriculture, Iwate University, Morioka, Japan).

Rabbit polyclonal antibodies (IgG) against M and HN were generated by Hokkaido System Science Co. Ltd. (Sapporo, Japan), using peptide antigens of HN and M. The peptide sequence of HN was 276-VDERTDYSSDGIED-289, and that of M was 23-LRTGPDKKAIPHIR-36.

2.3. Cell culture

Monkey kidney cells (LLCMK2) were maintained in minimum essential medium (MEM) (Gibco-BRL, Rockville, MD, USA), and Baby hamster kidney cells (BHK-21) and normal embryonic mouse liver cells (BNL-CL2) were maintained in Dulbecco's modified Eagle's medium (DMEM) (Nacalai Tesque Inc., Tokyo, Japan). Both MEM and DMEM were supplemented with 10% fetal bovine serum (FBS) (Biowest, Nuaillé, France), 100 units/ml penicillin and 0.1 mg/ml streptomycin (Penicillin–Streptomycin Mixed Solution) (Nacalai Tesque Inc.).

2.4. siRNA synthesis for HN mRNA knock-down

Five siRNAs for HN mRNA knock-down were designed and synthesized using SMART siRNA Technology™ at Dharmacon Research (Dharmacon, Lafayette, CO, USA). Each siRNA (HN-223, -342, -899, -1142 and -1427) targeted a different sequence: GCAUUGAACAUGAGCAGCA (HN mRNA nucleotides 223–241), GAACAAAAACAGCAGGGAU (342–360), GAACUAAGUCUCACCGGUA (899–917), GCGUGAUCAUCCAGGUCAA (1142–1160), and GCGUAUACACUGAUGCUUA (1427–1447). Scramble siRNA for use as a control had a random sequence (GCGCGCUUUGUAGGAUUCG).

2.5. Transfection of culture cells with siRNA

Synthesized siRNAs were transferred to LLCMK2 cells at concentrations of 50, 100, 200 or 320 pmol/ml using Lipofectamin Reagent™ (Invitrogen, California, USA) and Plus Reagent (Invitrogen), according to the manufacturer's instructions.

2.6. Infection of culture cells with HVJ

After washing culture cells (LLCMK2, BHK and BNL-CL2) with Dulbecco's phosphate-buffered saline (PBS) (Nacalai Tesque Inc.), Opti-MEM I (GIBCO™, Invitrogen) containing different amounts of HVJ was added to the cells in order to determine the optimum particle numbers (0.06–3.0 particles/cell), and cells were infected with HVJ for 1 h under 5% CO_2 at 37 °C. The infection medium was then removed, and infected cells were washed with PBS, followed by incubation in culture medium for 24 h under 5% CO_2 at 37 °C.

2.7. Isolation of HN-depleted HVJ

LLCMK2 cells transfected with HN-899 or scramble siRNA at 100 pmol/ml by Lipofectamin Reagent and Plus Reagent for 24 h, were infected with HVJ (1.5 particles/cell) for 1 h. Untransfected control cells were subjected to the same procedure. Infected cells were then cultured in MEM containing 100 units/ml penicillin and 0.1 mg/ml streptomycin for 48 h, and culture medium was passed through a filter (pore size, 1.2 μm). The supernatant was centrifuged at 100,000 × g for 2 h at 4 °C to precipitate HVJ particles.

2.8. Quantification of viral genome by RT-PCR

HVJ RNA genomes were isolated using the PURESCRIPT® Cell and Tissue RNA Purification Trial Kit (Gentra Systems Inc., Minneapolis, MN, USA). cDNA was synthesized from the purified HVJ RNA genome (about 200 ng) using the SuperScript™ III First Strand Synthesis System (Invitrogen). HVJ genome (about 250 ng of cDNA) was quantified by real-time RT-PCR using the TaqMan® Universal PCR Master Mix (Applied Biosystems Japan Ltd., Tokyo, Japan) and TaqMan® MGB Probe (Applied Biosystems Japan Ltd.). The TaqMan MGB Probe (5′-FAM-ATCCACCTAGCAGCTGT-MGB-3′) recognized the L protein coding region of the HVJ genome.

2.9. Northern blotting

Total RNA was extracted from culture cells using the RNeasy Mini Kit (Qiagen K.K., Tokyo, Japan). Total RNA (30 μg) was electrophoresed on a 1% agarose gel (Cambrex Bio Science Rockland Inc., Rockland, MD, USA), and was transferred to a Hybond-N+ nylon transfer membrane (Amersham Biosciences UK Ltd., Buckinghamshire, UK). In order to detect HN, F, M and G3PDH mRNA in the membrane, hybridization was performed with ^{32}P-labeled cDNA probes using the Random Primers DNA Labeling System (Invitrogen) in PerfectHyb™ (Toyobo Co. Ltd., Osaka, Japan).

2.10. Western blotting

HVJ (about 6×10^7 particles) dissolved in sample buffer (125 mM Tris–HCl (pH 6.8), 10% 2-mercaptoethanol, 4% sodium dodecylsulfate, 10% sucrose, 0.004% bromophenol

blue) were subjected to SDS-PAGE on a 12% gel, and proteins were transferred to an Immobilon-P Transfer Membrane (Millipore Co, Billerica, MA, USA). After transfer, the membrane was incubated for 1 h with blocking buffer [5% skim milk (Nacalai Tesque Inc.) in wash buffer (2 mM Tris–HCl (pH 8.0), 342.2 mM sodium chloride, 0.05% Tween 20)], followed by incubation for 1 h with blocking buffer containing anti-HN, -F or -M IgG as primary antibodies. After treatment with primary antibodies, the membrane was washed with wash buffer and incubated for 1 h with blocking buffer containing ECL™ anti-rabbit IgG, horseradish peroxidase-linked whole antibody (from donkey) (Amersham Biosciences) for HN and M staining, or ECL™ anti-mouse IgG, horseradish peroxidase-linked whole antibody (from sheep) (Amersham Biosciences) for F staining as secondary antibodies. The membrane was washed with wash buffer, and ECL Western Blotting Detection Reagent (Amersham Biosciences) was used to detect the signals for each protein.

2.11. Hemagglutinating activity assay

Serial twofold dilutions of a 50-μl HVJ suspension from LLCMK2 cells untreated or treated with HN-899 siRNA or scramble siRNA were mixed in 96-well U-bottom plates. A 1% suspension of chick red blood cells (50 μl) was added to each well, followed by incubation for 1 h at 4 °C. Hemagglutination in each well was then observed, and the hemagglutinating titer [hemagglutinating assay unit (HAU)/ml] was calculated (Watanabe and Okada, 1974).

2.12. Measurement of infection ratio

LLCMK2, BHK-21 and BNL-CL2 cells were infected with cell-derived normal HVJ or HN-depleted HVJ (3 particles/cell), and incubated for 24 h after infection. Infected cells were fixed with 4% paraformaldehyde in PBS and treated with 0.1% Triton X in PBS. After blocking with 5% skim milk in PBS, cells were treated with anti-F monoclonal antibody f236 as a primary antibody. Cells were then washed with PBS, followed by treatment with Alexa Fluor 488 goat anti-mouse IgG antibody (Molecular Probes, Eugene, OR). Infected cells were detected by immunostaining of F protein synthesized in the cells under 200× magnification, and infection efficiency was calculated as the ratio of F-positive cells to total cells in a microscopic field.

2.13. Infection of HN-depleted HVJ and inhibition by anti-F antibody

LLCMK2 cells were seeded onto 24-well plates (4×10^4 cells/well) and were incubated under 5% CO_2 at 37 °C. To activate F protein, cell-derived HVJ (normal and HN-depleted) (7.5×10^6 particles/ml Opti-MEM) was treated with trypsin (5 μg/ml) for 1 h. HN-depleted HVJ was then treated with anti-F serum (including anti-F neutralizing antibody), preimmune serum or nothing at 37 °C for 30 min. Anti-F antibody concentration in the antiserum was approximately 30 μg/ml, and anti-F and preimmune serum was used at 25 μl/ml. These mixtures of HVJ and serum were added to cultured cells (56.25×10^6 particles/200 μl/well), which were then centrifuged at 500, 1000 or $2000 \times g$ for 10 min at 35 °C, followed by incubation under 5% CO_2 for 20 min at 37 °C. An uncentrifuged ($1 \times g$) sample was also prepared by incubating cells with cell-derived normal HVJ (56.25×10^6 particles/200 μl/well) for 30 min at 37 °C. Expression of F protein was analyzed with anti-F antibody at 24 h after infection.

2.14. Transfection of FITC-ODN using HN-depleted HVJ

LLCMK2 cells were seeded onto 24-well plates (4×10^4 cells/well) and incubated under 5% CO_2 at 37 °C. To inactivate HVJ, an HVJ suspension of 6.0×10^8 virus particles was irradiated with UV (99 mJ/cm^2). Inactivated HVJ that was unable to replicate is referred to as HVJ-E. In order to activate F protein, HVJ-E (normal and HN-depleted) (6.0×10^8 particles/ml PBS) was treated with trypsin (5 μg/ml) for 1 h. HVJ-E was then precipitated by centrifugation at $20{,}000 \times g$ for 10 min at 4 °C. Supernatant was discarded and the pellet was re-suspended in 200 μl PBS. FITC-labeled oligodeoxynucleotides (FITC-ODN) with a randomized sequence (5′-FITC-TTGCCGTACCTGACTTAGCC-3′) was purchased from Gene Design Inc. (Osaka, Japan), and was diluted in TE buffer to a concentration of 200 pmol/μl (Morishita et al., 1997). To ensure that FITC-ODN was enclosed in HVJ-E (Ito et al., 2005), FITC-ODN (200 pmol/10 μl PBS) and poly-L-Lysine (Sigma–Aldrich Japan K.K., Tokyo, Japan) (20 μg/20 μl PBS) were mixed (Flexman et al., 2005) and incubated for 10 min at room temperature. HVJ-E (normal and HN-depleted) (3×10^7 particles/10 μl PBS) and 0.08 μl Triton X (final 0.2%) were added to the mixture of FITC-ODN and poly-L-Lysine, which was then incubated for 5 min on ice. As a negative control, the mixture without HVJ-E was prepared. The mixture was centrifuged at $18{,}500 \times g$ for 5 min at 4 °C, the supernatant was discarded and the pellet was re-suspended in 200 μl Opti-MEM. The suspension of HN-depleted HVJ-E containing FITC-ODN was added to cultured cells (3×10^7 particles/200 μl/well), which were then centrifuged at $2000 \times g$ for 10 min at 35 °C, followed by incubation under 5% CO_2 for 50 min at 37 °C. An uncentrifuged ($1 \times g$) sample was also prepared by incubating cells with cell-derived normal HVJ-E and HN-depleted HVJ-E (3×10^7 particles/200 μl/well) for 60 min at 37 °C. After incubation, HVJ-E-treated cells were washed with PBS and added to culture medium, after which FITC in the cells was observed at 2 h after introduction.

3. Results

We hypothesized that when cells receiving HN-specific siRNA were infected with wild-type HVJ, viral production would be normal, despite the inhibited HN production.

3.1. Functional analysis of HN-siRNA

Five different siRNAs were evaluated for their suppression of HN mRNA (Fig. 1A). These siRNAs (HN-223, -342, -899, -1142, -1427) or scramble siRNA were introduced into LLCMK2 cells at 200 pmol/ml, and the cells were then infected with HVJ (0.06 particles/cell) after 24 h. HN mRNA after infection was detected by Northern blotting, and the lowest HN mRNA levels were obtained with HN-899 siRNA (HN-899).

We then optimized the timing of HVJ infection. After the introduction of HN-899 at 100 pmol/ml into LLCMK2 cells, cells were infected with HVJ (0.06 particles/cell) at 12, 24, 48 or 72 h after siRNA introduction, and HN mRNA at 24 h after infection was detected by Northern blotting. As shown in Fig. 1B, the largest inhibition of HN mRNA was obtained at 24 h after siRNA delivery; production subsequently increased. The most effective concentration of HN-899 was also optimized by introducing different concentrations of HN-899 (50, 100, 200 and 320 pmol/ml), and the ideal range was found to be from 100 to 200 pmol/ml (data not shown).

3.2. Specificity of HN mRNA knock-down effect by HN-siRNA

In order to investigate the specificity of HN mRNA knock-down by HN-899, levels of HN, F and M mRNA in cells treated with HN-899 at 100 pmol/ml and infected with HVJ (0.06 particles/cell) 24 h after siRNA treatment were analyzed by Northern blotting (Fig. 1C). Although HN mRNA levels decreased markedly, F and M mRNA levels were higher than those of scramble-siRNA-treated cells.

3.3. Protein constitution and function of HVJ derived from HN-siRNA-treated cells

We investigated the protein constitution and function of HVJ generated by HN-siRNA-treated cells. LLCMK2 cells was transfected with HN-899, and then infected with HVJ at 24 h after transfection. HVJ produced from the cells were then collected from culture medium at 48 h after infection, and proteins (HN, F and M) were detected by Western blotting. As seen in Fig. 2A, the amount of HN decreased markedly, but F and M proteins increased.

In order to examine whether this increase was a result of more viral particles or more viral proteins per particle, we calculated the particle number produced from infected cells. Although we have previously estimated the HVJ particle number by HAU (Kaneda et al., 2002), this estimation was not suitable in HN-depleted HVJ, and thus the viral genome was quantified by real time RT-PCR. We found that the number of viral particles produced from infected cells increased approximately 10-fold on introduction of either HN-899 siRNA or scramble siRNA, as compared with untreated cells. Western blotting was performed using samples having the same amount of viral genome, which revealed that the amounts of F and M protein per HVJ particle did not increase compared with untreated cells (data not shown).

Hemagglutinating activity of HVJ samples was then analyzed by chick erythrocyte hemagglutination assay (Fig. 2B). HVJ (HN-899-, scramble siRNA-treated or untreated) was collected from the same number of cells, and HA titer was measured. In Fig. 2B, the total titer of HVJ produced from about 1×10^7 infected LLCMK2 cells is shown. HA activity decreased markedly in HN-899-treated HVJ, while no inhibition

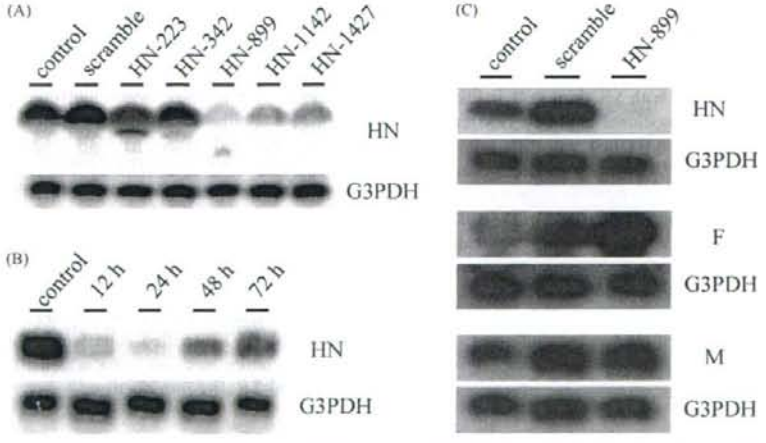

Fig. 1. Selection of optimum siRNA to knock-down HN mRNA. LLCMK2 cells received siRNA HN-223, -342, -899, -1142, -1427 or scramble siRNA (200 pmol/ml), and were infected with HVJ (0.06 particles/cell) at 24 h after siRNA introduction. Untransfected LLCMK2 cells infected with HVJ (0.06 particles/cell) were used as negative controls. (A) HN mRNA in the cells at 24 h after infection was detected by Northern blotting. HN-899 was found to induce the largest reductions in HN mRNA. (B) In order to investigate the optimum infection time of HVJ after siRNA induction, LLCMK2 cells were infected with HVJ at 12, 24, 48 and 72 h after HN-899 siRNA induction. The optimal infection time was found to be 24 h. (C) mRNA for HN, F and M in HN-899 siRNA-treated cells was analyzed by Northern blotting.

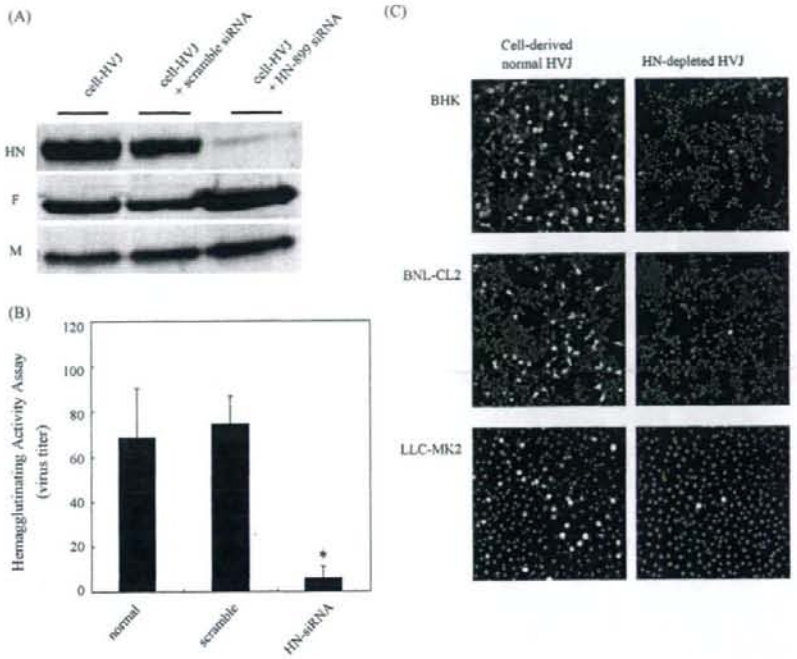

Fig. 2. Protein constitution and function of HVJ derived from HN-899 siRNA-treated cells. Untreated cells or cells treated with HN-899 siRNA or scramble siRNA (100 pmol/ml) were infected with HVJ (1.5 particles/cell), and progeny HVJ were collected from the culture medium after 48 h. (A) Western blots of HN, F and M protein of HVJ derived from untreated- (left), scramble-siRNA-treated (center) and HN-899-treated (right) cells. (B) Hemagglutinating activity assay of HVJ derived from untreated- (left), scramble-siRNA-treated (center) and HN-899-treated (right) cells. Data represent the means ± S.D. ($n = 5$). *$P < 0.05$ represents significant differences between the HN-siRNA treatment groups and controls. (C) Infection efficiency of normal HVJ or HN-depleted HVJ to LLCMK2, BHK-21 and BNL-CL2 cells, as evaluated by F protein expression. Blue dots are nuclei stained with DAPI, and green dots are F protein stained with Alexa 488. Labeled cells were visualized under 200× magnification.

was detected with scramble siRNA. Thus, HVJ with very low hemagglutinating activity was obtained with HN-899 siRNA treatment.

3.4. Infection efficiency of HN-depleted HVJ

We investigated the infection efficiencies of cell-derived normal HVJ and HN-depleted HVJ in BHK-21, BNL-CL2 and LLCMK2 cells (Fig. 4C). Cells were infected with cell-derived normal HVJ and HN-depleted HVJ (1.5×10^6 particles), and cells expressing F protein in the cytoplasm were detected by immunostaining for F protein. In all cell lines, the infection efficiency of HN-depleted HVJ was much lower than that of cell-derived normal HVJ.

3.5. Fusion ability of HN-depleted HVJ

Both HN and F proteins are required for cell fusion (Okada, 1993; Yeagle, 1993), and thus we examined whether HN-depleted HVJ could fuse with the cell membrane to complete viral infection. We hypothesized that fusion would occur provided that F could associate with lipid components in the membrane. Therefore, to induce its association with the lipid bilayer, viral infection was attempted both with and without centrifugation. As shown in Fig. 3A for LLCMK2 cells, HN-depleted HVJ infection, as evaluated by F protein expression, scarcely occurred without centrifugation ($1 \times g$). However, with centrifugation ($2000 \times g$), F-positive cells were frequently seen. Similar recovery of infectivity was observed in BNL-CL2 and BHK-21 (data not shown). As shown in Fig. 3B, the infection efficiency of HN-depleted HVJ at 1, 500, 1000 and $2000 \times g$ was approximately 10, 30, 70 and 80% of normal HVJ infection at $1 \times g$, respectively.

We next investigated whether the recovery of viral infection by centrifugation depended on the F protein in HN-depleted HVJ. Following treatment of HN-depleted HVJ with anti-F antibody rather than preimmune serum, F-positive cells were scarcely seen, even after $2000 \times g$ centrifugation (Fig. 3A) and, as shown in Fig. 3B, infection efficiency was strongly suppressed with anti-F antibody, while with preimmune serum, the efficiency was almost half of the level without antibody at all centrifugation speeds tested. These results suggest that HN-depleted HVJ retains its fusion ability derived from the F protein.

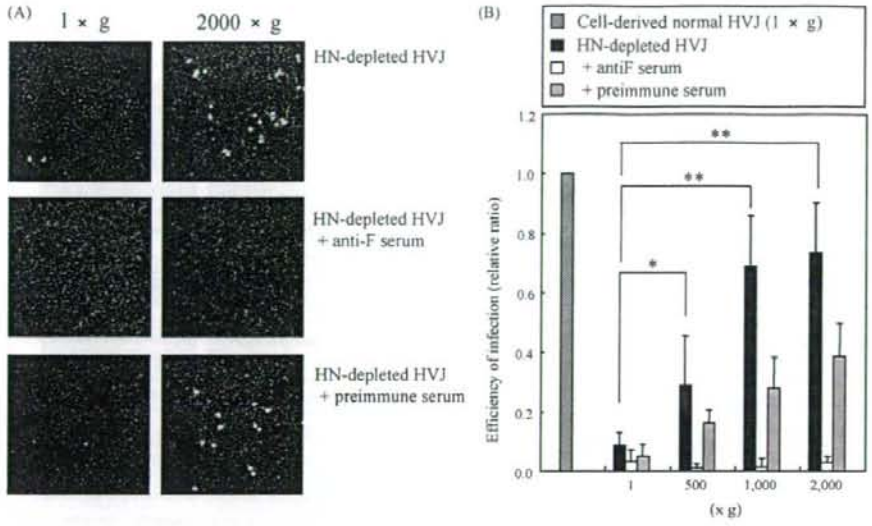

Fig. 3. Infection of cultured cells with HN-depleted HVJ. HN-depleted HVJ was treated with anti-F neutralizing serum, preimmune serum or PBS. HN-depleted HVJ was added to culture cells, and the mixture of cells and viruses was centrifuged at 500, 1000 or 2000 × *g*; 1 × *g* indicates treatment without centrifugation. (A) F protein expression on LLCMK2 cells was visualized under 100× magnification by immunofluorescence microscopy. Blue dots are nuclei stained with DAPI, and green dots are F protein stained with Alexa 488. (B) Infectivity of HN-depleted HVJ relative to that of cell-derived normal HVJ. Efficiency of infection was determined by the ratio of F-positive cells to all cells in a microscopic field. The infection efficiency of cell-derived normal HVJ at 1 × *g* is given as a standard value. Data represent means ± S.D. ($n = 8$). $^{*}P < 0.05$ and $^{**}P < 0.01$ represent significant differences between the HN-depleted HVJ groups with centrifugation at various speeds and without centrifugation.

3.6. Transfection ability of HN-depleted HVJ-E

We found that HN-depleted HVJ retains its fusion ability, but the suitability of HN-depleted HVJ as a delivery vector was uncertain. Therefore, we attempted to introduce FITC-ODN into LLCMK2 cells via HN-depleted HVJ (Fig. 4). HN-depleted HVJ and cell-derived normal HVJ were inactivated by UV irradiation. Inactivated HVJ that is unable to replicate is referred to as HVJ-E. FITC-ODN was enclosed in HN-depleted HVJ-E and normal HVJ-E, which were then added to LLCMK2 cells. The transfection efficiency of HN-depleted HVJ-E was lower than that of normal HVJ-E, as well as their infection efficiency, but was recovered with 2000 × *g* centrifugation (Fig. 4A and C). However, FITC-ODN was hardly introduced without HVJ-E at 2000 × *g* (Fig. 4C). Both normal HVJ-E and HN-depleted HVJ-E could introduce FITC-ODN into the cultured cells (Fig. 4B). These results suggest that HN-depleted HVJ is suitable for use as a delivery vector.

4. Discussion

We demonstrated the functional modification of HN activity on HVJ via a siRNA-mediated strategy.

We identified siRNA HN-899 as being able to inhibit HN mRNA after HVJ infection. Other siRNAs had some inhibitory effect on HN mRNA production, but the effect was less pronounced than when using HN-899. However, the inhibitory effects were transient (Fig. 1B), and the timing of HVJ infection after siRNA delivery was critical for effective inhibition. High and continuous production of mRNAs for viral proteins in HVJ-infected cells is apparently beyond the ability of RISC-mediated degradation of target mRNA by a single introduction of synthetic siRNA. To continue the inhibition of HN mRNA, stable expression of interfering RNA will be necessary. However, we have isolated stable transformants expressing interfering RNA containing the HN-899 sequence using a hairpin-type siRNA-producing plasmid (Brummelkamp et al., 2002).

Using HN-siRNA, HN protein was reduced markedly 24 h after HVJ infection (Fig. 2A), while F and M proteins increased as a result of elevated viral particle production rather than an increase in viral proteins per viral particle. These results suggest that treatment with HN-899 siRNA influences neither the viral protein contents of the new HVJ particles nor viral budding from HVJ-infected cells. We think that this method of virus modification is applicable to other envelope viruses, unless the effects of siRNA affect virus budding. However, it is likely that double-stranded short RNA increases the production of viral mRNA in HVJ-infected cells in a sequence-independent manner, as the mRNA of F and M also increased after the introduction of scramble siRNA. Therefore, a RISC-siRNA complex may accelerate the function of viral RNA-dependent RNA polymerase. Although the mechanism of the effects of siRNA on viral RNA production remains unknown, this method may be utilized for mass production of HVJ in cultured cells. It is necessary to test this phenomenon in other viruses.

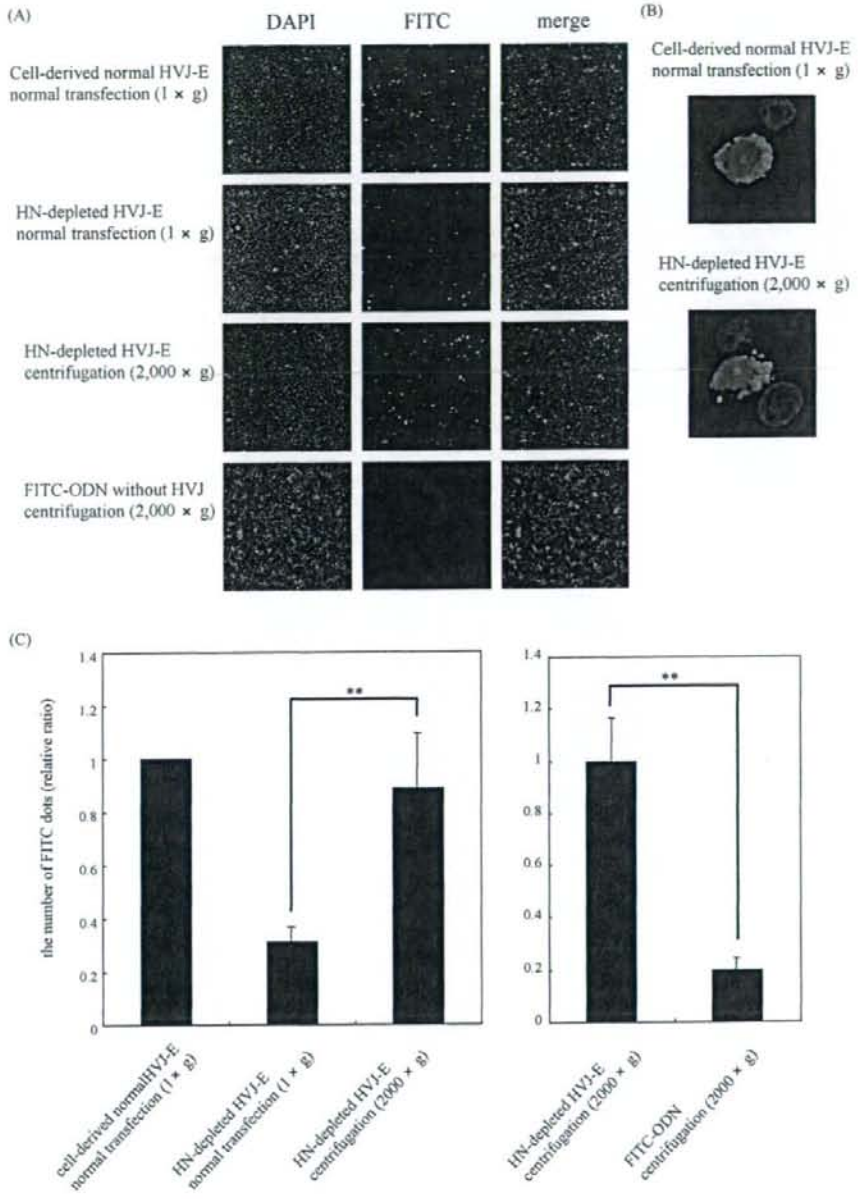

Fig. 4. Transfection of cultured cells with FITC-ODN using HN-depleted HVJ. HN-depleted HVJ and cell-derived normal HVJ were inactivated by UV irradiation (99 mJ/cm^2), and FITC-ODN was enclosed in them. HVJ-E containing FITC-ODN was added to culture cells, and (A) the transfected FITC-ODN was visualized under 100× magnification and (B) the intracellular localization of transfected FITC-ODN was visualized under 600× magnification by immunofluorescence microscopy. The mixture of cells and HN-depleted HVJ-E was centrifuged at 2000 × *g*, and FITC-ODN was visualized. Blue dots are nuclei stained with DAPI, and green dots are FITC-ODN. (C) Transfection efficiency of HN-depleted HVJ-E relative to that of cell-derived normal HVJ-E. Efficiency of transfection was determined by the number of dots of FITC in a microscopic field. The transfection efficiency of cell-derived normal HVJ at 1 × *g* is presented as a standard value. Data represent means ± S.D. ($n = 8$). $^{**}P < 0.01$ represents significant differences between the HN-depleted HVJ-E centrifuged at 2000 × *g* and uncentrifuged HN-depleted HVJ-E.

As expected, HN-depleted HVJ showed much lower hemagglutinating activity than wild-type HVJ, and we confirmed that viral infectivity was greatly attenuated without HN (Tanabayashi and Compans, 1996). We hypothesized that viral infection would be recovered when conditions were suitable for F to associate with the lipid bilayer of the cell membrane, as seen in the fusion of HVJ with liposomes (Mizuguchi et al., 1999). To test this, we attempted to infect cells with HN-depleted HVJ by centrifugation. Expression of F protein, an indicator of infectivity, increased with centrifugation speed, reaching approximately 80% of the infection efficiency of wild-type HVJ at 2000 × *g*. This increased infectivity was completely abrogated by preincubation with anti-F antibody. With preimmune serum, infectivity was approximately half that without serum. This inhibition might be due to the instability of HVJ in the presence of serum (Mima et al., 2005).

We also attempted the transfection of culture cells using HN-depleted HVJ-E in order to confirm that the modified HVJ-E is suitable for use as a delivery vector. Similarly to the infection test, the transfection efficiency of HN-depleted HVJ-E was lower than that of normal HVJ-E, but was recovered by 2000 × *g* centrifugation. Therefore, we believe that HN-depleted HVJ could be applied as a delivery vector.

However, centrifugation is obviously impractical for HN-depleted HVJ-based vectors, particularly for *in vivo* gene transfer or drug delivery, and thus we recently developed HVJ containing a tissue-targeting molecule on the envelope (Kawachi et al., 2007). A recombinant tissue-targeting protein was fused to the extracellular region of F protein by genetic engineering techniques. Cells expressing the recombinant protein were transfected with siRNA and infected with HVJ, and cell-derived HVJ containing the recombinant targeting protein and little HN was generated. When HN was depleted in the targeting HVJ using HN-899 siRNA, infection occurred normally at the cells recognized by the targeting molecule (Shimbo et al., 2007). This is consistent with a previous report, in which targeted delivery of oligonucleotides was achieved using antibody-conjugated HVJ-liposomes without being affected by HN protein (Tomita et al., 2002). Based on these results, the binding of HVJ to the cell membrane followed by endocytotic uptake may replace centrifugation to achieve normal infection of HN-depleted HVJ. Therefore, the use of tissue-targeting molecules will enable HN-depleted HVJ-based vectors to deliver therapeutic molecules to target cells.

Acknowledgments

This work was supported by grants from the Ministry of Health, Labour and Welfare and the Ministry of Economy, Trade and Industry of Japan.

References

Ali, A., Nayak, D.P., 2000. Assembly of Sendai virus: M protein interacts with F and HN proteins and with the cytoplasmic tail and transmembrane domain of F protein. Virology 276, 289–303.

Asano, K., Asano, A., 1988. Binding of cholesterol and inhibitory peptide derivatives with the fusogenic hydrophobic sequence of F-glycoprotein of HVJ (Sendai virus): possible implication in the fusion reaction. Biochemistry 27, 1321–1329.

Brummelkamp, T.R., Bernards, R., Agami, R., 2002. A system for stable expression of short interfering RNAs in mammalian cells. Science 296, 550–553.

Curran, J., Kolakofsky, D., 1999. Replication of paramyxoviruses. Adv. Virus Res. 54, 403–422.

Dallocchio, F., Tomasi, M., Bellini, T., 1995. Activation of the Sendai virus fusion protein by receptor binding. Biochem. Biophys. Res. Commun. 208, 36–41.

Flexman, J.A., Kim, Y., Miyoshi, S., Lewellen, B.L., Cross, D.J., Minoshima, S., 2005. A viral envelope as a vehicle for tracer, drug, and gene delivery: Initial biodistribution study using PET imaging. Conf. Proc. IEEE Eng. Med. Biol. Soc. 1, 793–796.

Hoekstra, D., Klappe, K., 1986. Sendai virus–erythrocyte membrane interaction: quantitative and kinetic analysis of viral binding, dissociation, and fusion. J. Virol. 58, 87–95.

Inoue, J., Nojima, S., Inoue, K., 1985. The activity of membranes reconstituted from HVJ envelope proteins and lipids to induce hemolysis and fusion between liposomes and erythrocytes. Biochim. Biophys. Acta 816, 321–331.

Ito, M., Yamamoto, S., Nimura, K., Hiraoka, K., Tamai, K., Kaneda, Y., 2005. Rad51 siRNA delivered by HVJ envelope vector enhances the anti-cancer effect of cisplatin. J. Gene Med. 7, 1044–1052.

Kaneda, Y., Nakajima, T., Nishikawa, T., Yamamoto, S., Ikegami, H., Suzuki, N., Nakamura, H., Morishita, R., Kotani, H., 2002. Hemagglutinating virus of Japan (HVJ) envelope vector as a versatile gene delivery system. Mol. Ther. 6, 219–226.

Kaneda, Y., Yamamoto, S., Nakajima, T., 2005. Development of HVJ envelope vector and its application to gene therapy. Adv. Genet. 53, 307–332.

Kawachi, M., Tamai, K., Saga, K., Yamazaki, T., Fujita, H., Shimbo, T., Kikuchi, Y., Nimura, K., Nishifuji, K., Amagai, M., Uitto, J., Kaneda, Y., 2007. Development of tissue-targeting hemagglutinating virus of Japan envelope vector for successful delivery of therapeutic gene to mouse skin. Hum Gene Ther. 18, 881–894.

Lamb, R.A., Kolakofsky, D., 2001. Paramyxoviridae: the viruses and their replication. In: Knipe, D.M., Howley, P.M. (Eds.), Fields Virology. Philadelphia, pp. 1305–1340.

Mima, H., Tomoshige, R., Kanamori, T., Tabata, Y., Yamamoto, S., Ito, S., Tamai, K., Kaneda, Y., 2005. Biocompatible polymer enhances the in vitro and in vivo transfection efficiency of HVJ envelope vector. J. Gene Med. 7, 888–897.

Mizuguchi, H., Nakanishi, T., Kondoh, M., Nakagawa, T., Nakanishi, M., Matsuyama, T., Tsutsumi, Y., Nakagawa, S., Mayumi, T., 1999. Fusion of Sendai virus with liposome depends on only F protein, but not HN protein. Virus Res. 59, 191–201.

Morishita, R., Sugimoto, T., Aoki, M., Kida, I., Tomita, N., Moriguchi, A., Maeda, K., Sawa, Y., Kaneda, Y., Higaki, J., Ogihara, T., 1997. In vivo transfection of *cis* element "decoy" against nuclear factor-kappaB binding site prevents myocardial infarction. Nat. Med. 3, 894–899.

Mottet, G., Muller, V., Roux, L., 1999. Characterization of Sendai virus M protein mutants that can partially interfere with virus particle production. J. Gen. Virol. 80 (Pt 11), 2977–2986.

Okada, Y., 1993. Sendai virus-induced cell fusion. Methods Enzymol. 221, 18–41.

Portner, A., Scroggs, R.A., Metzger, D.W., 1987. Distinct functions of antigenic sites of the HN glycoprotein of Sendai virus. Virology 158, 61–68.

Shimbo, T., Kawachi, M., Saga, K., Fujita, H., Yamazaki, T., Tamai, K., Kaneda, Y., 2007. Development of a transferrin receptor-targeting HVJ-E vector. Biochem. Biophys. Res. Comm. 364, 423–428.

Takimoto, T., Murti, K.G., Bousse, T., Scroggs, R.A., Portner, A., 2001. Role of matrix and fusion proteins in budding of Sendai virus. J. Virol. 75, 11384–11391.

Takimoto, T., Taylor, G.L., Connaris, H.C., Crennell, S.J., Portner, A., 2002. Role of the hemagglutinin-neuraminidase protein in the mechanism of paramyxovirus–cell membrane fusion. J. Virol. 76, 13028–13033.

Tanabayashi, K., Compans, R.W., 1996. Functional interaction of paramyxovirus glycoproteins: identification of a domain in Sendai virus HN which promotes cell fusion. J. Virol. 70, 6112–6118.

Tashiro, M., McQueen, N.L., Seto, J.T., 1999. Determinants of organ tropism of Sendai virus. Front. Biosci. 4, D642–D645.

Tomita, N., Morishita, R., Yamamoto, K., Higaki, J., Dzau, V.J., Ogihara, T., Kaneda, Y., 2002. Targeted gene therapy for rat glomerulonephritis using HVJ-immunoliposomes. J. Gene Med. 4, 527–535.

Tozawa, H., Komatsu, H., Ohkata, K., Nakajima, T., Watanabe, M., Tanaka, Y., Arifuku, M., 1986. Neutralizing activity of the antibodies against two kinds of envelope glycoproteins of Sendai virus. Arch. Virol. 91, 145–161.

Watanabe, K., Okada, Y., 1974. A new method for propagation of HVJ (Sendai virus) in vitro: high sensitivity and productivity in spreading cultures of fragmented chorioallantoic membrane of chick embryos. Biken. J. 17, 51–58.

Yeagle, P.L., 1993. The Fusion of Sendai Virus. CRC Press Inc., London.

suggested that opsin is expressed in the epidermis (data not shown).

Although the mechanisms involved have not been clarified, our findings indicate that visible light exerts wavelength-dependent effects upon epidermal barrier homeostasis.

MATERIALS AND METHODS

Materials

All experiments were performed on 7- to 10-week-old male hairless mice (HR-1, Hoshino, Japan). All procedures in the measurement of skin barrier function, disruption of the barrier, and application of test sample were carried out under anesthesia. All experiments were approved by the Animal Research Committee of the Shiseido Research Center in accordance with the National Research Council Guide (National Research Council, 1996).

Visible light radiation

To obtain radiation of each wavelength range, we used arrays of 50 light-emitting diodes (Nakamura 1998) (lamp type 5 mm series, Nichia, Tokushima, Japan). The power level was set at 20 W (W = joules of energy per second) with a variable resistor. Radiation was applied for 1 hour from the light-emitting diodes placed at 5 cm from the surface of the skin or skin section, immediately after barrier disruption by tape stripping (Denda *et al.*, 1998). During the radiation, the temperature at the surface of the skin or skin section was kept at 37°C by the use of a heat pad.

Cutaneous barrier function

Permeability barrier function was evaluated by measurement of transepidermal water loss with an electric water analyzer (Meeco, Warrington, PA) as described previously (Denda *et al.*, 2007).

Organ culture study

Immediately after euthanasia of hairless mice by pentobarbital application, flank skin (2 × 2 cm) was taken and the barrier was disrupted by acetone treatment as previously described (Denda *et al.* 1998). Then the skin sections were incubated with DMEM (Cellgro Mediatech, Herndon, VA) at 37°C under different conditions of light exposure for 1 hour. At the end of the incubation, the transepidermal water loss was evaluated and tissue was taken for electron-microscopic study.

Electron-microscopic study

Full-thickness skin samples for electron microscopy were cut into pieces ($<0.5\ mm^3$) and fixed overnight in modified Karnovsky's fixative. They were then post-fixed in 2% aqueous osmium tetroxide or 0.2% ruthenium tetroxide as described previously (Denda *et al.*, 1998). Parameters were evaluated from photographs of randomly selected sections at a constant magnification, using computer software (NIH Image).

Reverse transcription-PCR assays

We used four mice for the assay. Epidermis of the skin tissue was removed by incubation in a 10 mM EDTA phosphate-buffered saline solution at 37°C for 30 min and total RNA was isolated by ISOGEN (Wako, Osaka, Japan), containing phenol and guanidine thiocyanate, according to the manufacturer's instructions. The resulting pellet was suspended in 10 μl of water, and 2 μl was analyzed by PCR. For opsin5 analysis, primer 1 (AGTCTGTGATCTGGGG ATATCAGG region 228–402, 175 bp) and primer 2 (ACAGAT CTTCAG ATA GCGG TCCAG region 228–377, 150 bp).

Statistics

Results are expressed as the mean ± SD. The statistical significance of differences were determined by analysis of variance with Fisher's protected least significant difference.

CONFLICT OF INTEREST

The authors state no conflict of interest.

Mitsuhiro Denda[1] and Shigeyoshi Fuziwara[1]

[1]Shiseido Research Center, Life Science Research Center, 2-12-1, Fukuura, Kanazawa-ku, Yokohama, Japan
E-mail: mitsuhiro.denda@to.shiseido.co.jp

REFERENCES

Denda M, Sato J, Tsuchiya T, Elias PM, Feingold KR (1998) Low humidity stimulates epidermal DNA synthesis and amplifies the hyperproliferative response to barrier disruption: implication for seasonal exacerbations of inflammatory dermatoses. *J Invest Dermatol* 111:873–8

Denda M, Sokabe T, Tominaga-Fukumi T, Tominaga M (2007) Effects of skin surface temperature on epidermal permeability barrier homeostasis. *J Invest Dermatol* 127: 654–9

Nakamura S (1998) The role of structural imperfections in InGaN-based blue light-emitting diodes and laser diodes. *Science* 281:956–61

National Research Council (1996) *National Research Council (NRC) Guide.* National Academy Press, Washington

Identification of Skn-1n, a Splice Variant Induced by High Calcium Concentration and Specifically Expressed in Normal Human Keratinocytes

Journal of Investigative Dermatology (2008) **128,** 1336–1339; doi:10.1038/sj.jid.5701143; published online 8 November 2007

TO THE EDITOR

POU domain transcription factors are a superfamily of homeodomain proteins that regulate cell differentiation and proliferation (Scholer, 1991; Wegner *et al.*, 1993) in a promoter-dependent and cell type-specific manner. Three POU proteins, Oct-1, Oct-6, and *Skn-1a*, are known to be expressed in the epidermis. Among them, the *Skn-1a* gene is primarily, if not exclusively, expressed in the epidermis (Andersen

Abbreviations: RT-PCR, reverse transcription-PCR; NHEK, normal human epidermal keratinocyte

et al., 1993). Previous *in vitro* studies demonstrated that Skn-1a binds to and transactivates the promoter regions of keratinocyte genes involved in epidermal differentiation, such as human keratin 10 (Andersen *et al.*, 1993) and *SPRR-2A* (Fischer *et al.*, 1996). Thus, Skn-1a appears to regulate, both temporally and spatially, the expression of keratinocyte-specific genes during differentiation, playing a role in the development and differentiation of the epidermis. In this study, we provide early evidence for an alternative splice variant Skn-1n that is induced by high calcium concentration and specifically expressed in normal human epidermal keratinocytes.

To determine the 5′ end of Skn-1a mRNA, 5′ rapid amplification of cDNA ends PCR was performed and two bands of PCR product in the 300–400 bp range were noted (Figure 1). The shorter rapid amplification of cDNA ends product was specifically shown to contain the 5′ end of Skn-1a cDNA by direct sequence. Sequencing of the longer rapid amplification of cDNA ends product revealed that there was a 112-bp insertion in the cDNA sequence when compared with the published human Skn-1a cDNA sequence (GenBank accession no. AF162278, Figure 1b). This cDNA clone, designated as Skn-1n, contained two in-frame translational start sites, one at nucleotide position −124 (distal ATG codon) and the other at the position 1 (proximal ATG codon). However, the use of the distal ATG codon in Skn-1n created a termination codon at −42, while if the proximal ATG codon was used, it is predicted to create an open-reading frame of 432 amino acids. Reverse transcription-PCR (RT-PCR) was used to clone the full-length human Skn-1n cDNA. Comparison of open-reading frame of both Skn-1n and Skn-1a revealed that the deduced N-terminus of Skn-1n was shorter than the N-terminus of Skn-1a by four amino-acid residues, while downstream of the N-terminus of Skn-1n the sequences were identical with

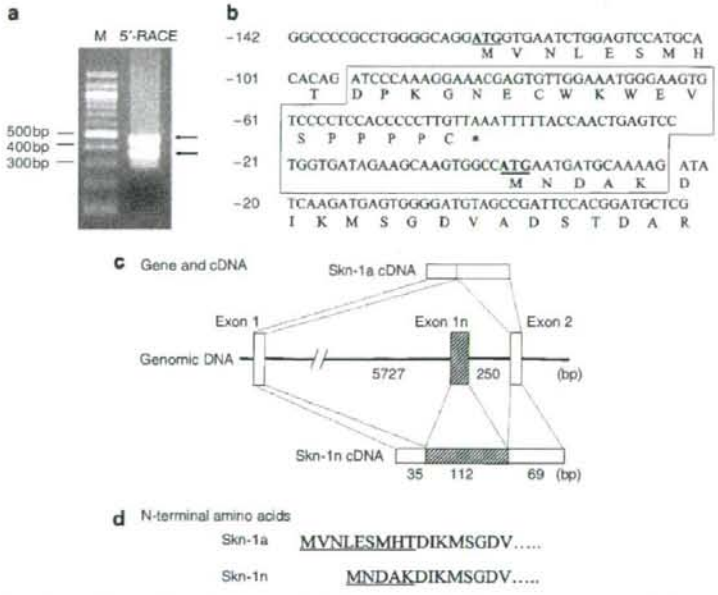

Figure 1. Identification of a splice variant Skn-1n. (**a**) 5′Rapid amplification of cDNA ends of human Skn-1a was performed using 5′-rapid amplification of cDNA ends System for Rapid Amplification of cDNA Ends, Version 2.0 (Life Technologies, Gaithersburg, MD) according to the instruction manual. The Skn-1a cDNA was reverse transcribed from 1 μg total NHEK RNA using a gene-specific primer (5′-GAGACCGCTTTGTTGCTGTG-3′) corresponding to position 503–527 of the Skn-1a mRNA, and subjected to PCR. Using the PCR products, the secondary PCR with the supplied anchor primer and nested gene-specific primer (5′-GGTTTCCGGACATCATGGCAGGTCCTT-3′) was performed. The PCR products were separated by 1.5% agarose gel electrophoresis and visualized with ethidium bromide. The major two bands were indicated by arrows. M, molecular weight marker. (**b**) To isolate a full-length Skn-1n clone, we performed RT-PCR using total RNA prepared from NHEK. The resultant cDNA was amplified with primer pairs specific for Skn-1n: sense primer (5′-CGAGTGTTGGAAATG GGAAGT-3′) and antisense primer (5′-AAAATGGGGTGAGATGAAGAT-3′), followed by the secondary PCR with nested sense primer (5′-CTGAGTCCTGG TGATAGAAGC-3′) and nested antisense primer (5′-AGGAAGGTGAAAATGGTAAGC-3′). The PCR products were subcloned and sequenced with a DNA analyzer. Numbers to the left of each row of the nucleotide sequence refer to the nucleotide position. The distal ATG codon (at nucleotide position −124) is underlined and the proximal ATG codon (at nucleotide position +1) is double underlined. Asterisk, a termination codon (TAA) at nucleotide position −42. The alternatively spliced exon 1n is boxed. (**c**) The human *Skn-1a* genomic organization is depicted schematically with the exon shown as boxes and the intron shown as horizontal lines. The exon 1n is shown as a hatched box. (**d**) Comparison of deduced amino-acid sequences of Skn-1a and Skn-1n. The differences in the amino-terminal sequences of the two proteins are highlighted by underlining.

that of Skn-1a (Figure 1b and d). Comparison of the Skn-1a and Skn-1n cDNA sequences with those in the genomic DNA revealed that the 112-bp insert detected in Skn-1n is encoded by sequences embedded within the intron 1 (Figure 1c). The exon within the Skn-1a gene is designated as exon 1n (Figure 1c). Thus, Skn-1n is an alternative splice variant resulting in generation of a protein different of Skn-1a due to utilization of a different translation initiation codon (Figure 1b and c). This variant is distinct from the previously identified Skn-1 isoforms, the human Skn1d1 and Skn1d2 (Cabral et al., 2003) and the mouse Skn-1i (Andersen *et al.*, 1993).

Both Skn-1a and Skn-1n transcripts were specifically expressed in normal human epidermal keratinocytes (NHEK), but not detected in the immortalized human keratinocytes HaCaT, or in the selected cell lines (Figure 2a). The absence of Skn-1a expression in HaCaT is in agreement with the previous data (Hildesheim *et al.*, 1999). This keratinocyte cell line is known to maintain some characteristics of the terminal differentiation of epidermis, such as keratinization and involucrin induction. Interestingly, Skn-1a knockout mice do not exhibit obvious phenotypic changes in the skin (Andersen *et al.*, 1997). These findings suggest that Skn-1 is not prerequisite for the terminal differentiation of epidermal keratinocytes and that there are compensatory POU molecules for coordinated differentiation of the epidermis. Indeed, double knockout of Skn-1a and Oct-6, another POU member expressed in the skin, resulted in abnormal differentiation and wound healing of the epidermis (Andersen *et al.*, 1997). Semiquantitative RT-PCR analysis showed that the relative amount of Skn-1a mRNA was higher than that of Skn-1n, implying that the former is predominately expressed in NHEK (Figure 2b). In NHEK cultured with the high calcium concentrations for 48 hours, the level of Skn-1a expression was approximately 25-fold higher than that in cells with low calcium (Figure 2c, upper panel). This is consistent with the previous *in vivo* and *in vitro* studies (Andersen *et al.*, 1997; Cabral *et al.*, 2003). The Skn-1n mRNA level was also significantly increased in NHEK stimulated with high calcium (Figure 2c, middle panel). Although the precise function of these epidermal-specific POU transcription factors remains to be clarified, genetic alterations of these factors may cause congenital epidermal diseases reflecting disorganized epidermogenesis. In this context, cloning and characterization of the structures of epidermal POU genes should enhance our ability to identify such skin diseases.

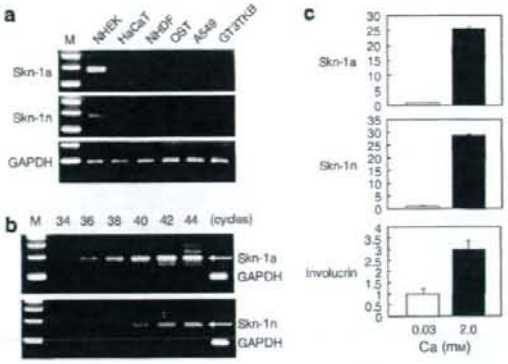

Figure 2. Effect of high calcium concentration on the expression of Skn-1a and -1n transcripts in NHEK. (**a**) RT-PCR analysis of Skn-1a, Skn-1n, and glyceraldehyde-3-phosphate dehydrogenase expression in various human cultured cells. The primers for detection of Skn-1a and Skn-1n transcripts, designed with OLIGO Analysis Software (Molecular Biology Insights, Cascade, CO), were as follows: Skn-1a: forward: 5′-GAGTCCATGCACACAGATAT-3′, reverse: 5′-ATGGCCGATGGGAGAGGGTC-3′ (product size; 175 bp). Skn-1n: forward: 5′-GTCCCCTCCACCCCCTTGTT-3′, reverse: TCTAGGCCATTTCGATCATT (product size; 169 bp). cDNA was prepared by reverse transcription of 0.5 μg total RNA. PCR was performed with 40 cycles. NHEK, normal human epidermal keratinocytes; HaCaT, spontaneously immortalized human keratinocyte cell line; OST, human osteosarcoma cell line; NHDF, normal human dermal fibroblasts; A549, human lung carcinoma cell line; GT3TKB, human gastric adenocarcinoma cell line; M, molecular weight marker. (**b**) Semiquantitative RT-PCR analysis of Skn-1a and Skn-1n expression in NHEK. Reverse transcription and PCR were performed as described above with 34-44 PCR cycles. For glyceraldehyde-3-phosphate dehydrogenase, only the 40-cycle product is shown. (**c**) Skn-1a and Skn-1n mRNA expression in NHEK cultured in low (0.03 mM) and high (2.0 mM) calcium-containing medium was determined by quantitative real-time RT-PCR analysis. Total RNA was extracted from keratinocytes using the RNeasy kit (Qiagen, Hilden, Germany). cDNA was prepared by reverse transcription of 0.5 μg total RNA. The primers used to detect the expression levels of Skn-1a, Skn-1n, and involucrin transcripts, designed with OLIGO Analysis Software, were as follows: Skn-1a: forward: 5′-GAGTCCATGCACAC AGATAT-3′, reverse: 5′-TCTAGGCCATTTCGATCATT-3′. Skn-1n: the same primer pair as (**a**). Involucrin: forward: 5′-CCAGTCAATACCCATCAGGA-3′, reverse: 5′-CCTTTACAGCAGTCATGTGC-3′. Continuous quantitative measurement of the PCR products was achieved by incorporation of SYBR Green fluorescent dye (Opticon 2, Bio-Rad, Hercules, CA). All real-time PCR were performed in triplicate. The transcript level of each gene was normalized to the corresponding glyceraldehyde-3-phosphate dehydrogenase. The results are expressed as mean ± SD. Data are representative of three independent experiments.

This study protocol was approved by the Institutional Review Board.

CONFLICT OF INTEREST

The authors state no conflict of interest.

ACKNOWLEDGMENTS

We thank Yoko Chiba and Carol Kelly for assistance. This study was supported by grants from the Ministry of Health, Labour and Welfare of Japan (13778128), the Ministry of Education, Culture, Sports, Science and Technology of Japan (10479185), Karouji Memorial Foundation, and Takeda Foundation, as well as by grants from the National Institutes of Health (P01 AR38923).

Koji Nakajima[1], Katsuto Tamai[2], Takehiko Yamazaki[1], Yuka Toyomaki[1], Hajime Nakano[1], Jouni Uitto[3] and Daisuke Sawamura[1]

[1]Department of Dermatology, Hirosaki University School of Medicine, Hirosaki, Japan; [2]Division of Gene Therapy Science, Osaka University Graduate School of Medicine, Osaka, Japan and [3]Department of Dermatology and Cutaneous Biology, Jefferson Medical College, Thomas Jefferson University, PA, USA
E-mail: hnakano@cc.hirosaki-u.ac.jp

REFERENCES

Andersen B, Schonemann MD, Flynn SE, Pearse RV, Singh H, Rosenfeld MG (1993) Skn-1a and Skn-1i: two functionally distinct Oct-2-related factors expressed in epidermis. *Science* 260:78–82

Andersen B, Weinberg WC, Rennekampff O, McEvilly RJ, Bermingham JR Jr, Hooshmand F *et al.* (1997) Functions of the POU domain genes Skn-1a/i and Tst-1/Oct-6/SCIP in epidermal differentiation. *Genes Dev* 11: 1873–84

Cabral A, Fischer DF, Vermeij WP, Backendorf C (2003) Distinct functional interactions of human Skn-1 isoforms with Ese-1 during keratinocyte differentiation. *J Biol Chem* 278:17792–9

Fischer DF, Gibbs S, van De Putte P, Backendorf C (1996) Interdependent transcription control elements regulate the expression of the SPRR2A gene during keratinocyte terminal differentiation. *Mol Cell Biol* 16:5365–74

Hildesheim J, Foster RA, Chamberlin ME, Vogel JC (1999) Characterization of the regulatory domains of the human skn-1a/Epoc-1/Oct-11 POU transcription factor. *J Biol Chem* 274:26399–406

Scholer HR (1991) Octamania: the POU factors in murine development. *Trends Genet* 7: 323–9

Wegner M, Drolet DW, Rosenfeld MG (1993) POU-domain proteins: structure and function of developmental regulators. *Curr Opin Cell Biol* 5:488–98